axioms

IMPACT FACTOR 1.6

Article

The Fine-Structure Constant in the Bivector Standard Model

Bryan Sanctuary

Special Issue
Mathematical Aspects of Quantum Field Theory and Quantization

Edited by
Dr. Alexandre Landry

MDPI

https://doi.org/10.3390/axioms14110841

axioms

MDPI

Article

The Fine-Structure Constant in the Bivector Standard Model

Bryan Sanctuary †

Department of Chemistry, McGill University, Montreal, QC H3A 0B8, Canada; bryan.sanctuary@mcgill.ca
† Retired Professor.

Abstract

The geometrical view of the electron as a spinning bivector leads to the partitioning of the electron's energy into internal and external. The reduced Compton wavelength, $\bar{\lambda}_C$, is taken as the radius of the inertial ring (a disc), while r_e characterizes the EM coupling scale. Within this picture, the fine-structure constant emerges as the structural ratio $\alpha = r_e/\bar{\lambda}_C$. We make the partitioning explicit, derive simple ratios among moments of inertia and stored energies, and compare the Bivector Standard Model with the Standard model.

Keywords: fine structure constant; classical spin; geometric algebra; classical correspondence; coherence; parity; reflection; quantum theory; standard model; bivector standard model

MSC: 81-10

1. Introduction

The fine-structure constant (FSC) $\alpha \approx 1/137$ is a dimensionless measure of electromagnetic coupling that pervades atomic physics and quantum electrodynamics, yet its origin remains obscure. From Eddington, ref. [1] and Dirac [2] to Feynman [3,4] and the latest measurements [5–7], there is still no accepted first-principles derivation within the point-particle electron paradigm of the Standard Model (SM).

In this work, we explore an alternative geometric description in which the electron's spin is modeled as a bivector, [8,9]. It has two massive, orthogonal axes forming a rigid rotor that precesses about a third axis. This is illustrated in Figure 1, left panel, and arises naturally in a geometric–algebra (GA) formulation, [10], with a different metric signature than the usual SM spinor representation. This establishes a new Bivector SM (BiSM) [9]. Figure 2 contrasts the usual SM with the BiSM: the former gives Dirac's matter—antimatter pair; and the latter gives two counter-precessing angular-momentum cones on a single particle.

The key claim is structural and classical: the bivector rotor partitions the electron's energy between an external, field-coupled motion in the Laboratory Fixed Frame (LFF), and an internal, mass-like motion in the Body Fixed Frame (BFF). We show that this partition can be expressed as follows,

$$\alpha = \frac{E^{\mathrm{LFF}}_{\mathrm{external}}}{E^{\mathrm{LFF}}_{\mathrm{external}} + E^{\mathrm{BFF}}_{\mathrm{internal}}} = \frac{I_V}{I_V + 4I_B}, \tag{1}$$

for a rigid bivector with external vector and internal bivector inertias, I_V and I_B, where the factor of 4 reflects the doubled precession frequency of the internal blades [10]. We then recover the usual relation,

check for updates

Academic Editor: Alexandre Landry

Received: 20 October 2025
Revised: 8 November 2025
Accepted: 11 November 2025
Published: 17 November 2025

Citation: Sanctuary, B. The Fine-Structure Constant in the Bivector Standard Model. *Axioms* **2025**, *14*, 841. https://doi.org/10.3390/axioms14110841

$$\alpha = \frac{r_e}{\bar{\lambda}_C} \tag{2}$$

and identify the reduced Compton wavelength [11], $\bar{\lambda}_C$, as the radius of the inertial ring and r_e as the electromagnetic coupling scale of the same geometry. Together, these relations interpret α as a fixed structural ratio that quantifies how only a small fraction of the electron's content is directly available for electromagnetic coupling.

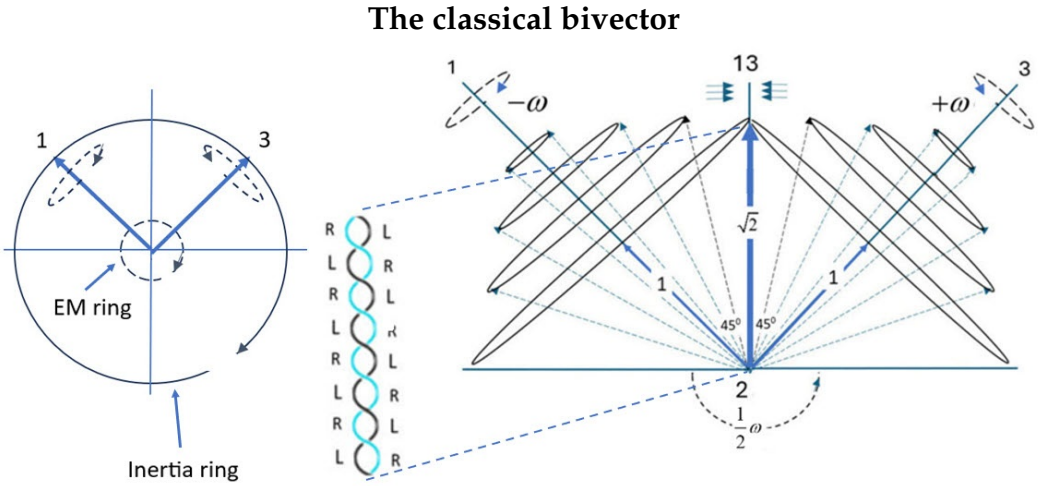

Figure 1. Classical spin's bifurcation from reflection to parity. From Left to Right: 1. Bivector electron as a rotor: body-fixed blades along e_1, e_3 precess about e_2. The inertial ring has radius $R = \bar{\lambda}_C$; the EM-coupling rim is characterized by r_e. 2. The details of the double helix with left and right reflection intertwined. 3. The two mirror-image precession states, $\psi^{\pm}$, represent Nature's left and right hands by L and R hand rules. The angles between axes 1 and 3 and their angular momentum vectors are equal in both states and increase with precession frequency. As $\Phi \to 0$, the double helix forms within the 13 reflection plane. This is the quantum domain.

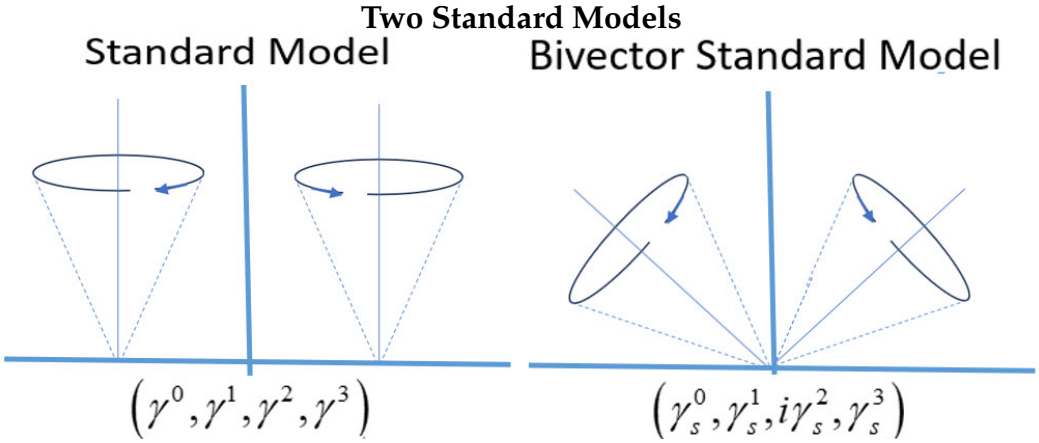

Figure 2. Left: Dirac's matter–antimatter pair of the SM with Clifford algebra $Cl(1,3)$. Right: The BiSM, showing two counter-precessing angular momentum cones on the same particle, forming a bivector with $Cl(2,2)$.

Scope and Goals

The objective is to establish that the FSC emerges as a structural ratio in the BiSM geometry. Since the FSC is the basis for broader topics, we restrict the discussion to this, and defer application to when the internal dynamics of the bivector are developed. There, we discuss applications such as the Zitterbewegung, zbw [12], the double slit analysis, g-factor correction, spectra, and radiative shifts. Here, we focus only on the geometric origin of α,

and provide one illustrative example. These applications are aimed to show that the BiSM is numerically equivalent to the SM, but offers a deeper geometric interpretation with a classical correspondence.

2. The Bivector Electron

The two massive, orthogonal axes, 1 and 3, define an internal plane 13, which is orthogonal to the linear–momentum axis 2. This can spin with either helicity, as shown in Figure 1, left panel [9]. An external torque about axis 2 transfers angular momentum into the internal BFF, producing a centrifugal force along the 13 bisector. In response, cones of angular momentum form around each axis; they counter-precess at a frequency that is twice that of the external torque about axis 2. This is a geometric realisation of the SU(2) double cover over SO(3).

In GA the classical spin bivector is the wedge of the two angular-momentum vectors associated with the internal axes [9],

$$B = \mathbf{S}_1 \wedge \mathbf{S}_3. \tag{3}$$

Euler's equations [13] for a rigid body in the interaction plane 13 yield,

$$\begin{aligned} \mathbf{S}_3 &= e^{+31}\cos\frac{\Phi}{2} + e^{-31}\sin\frac{\Phi}{2}, \\ \mathbf{S}_1 &= e^{+31}\cos\frac{\Phi}{2} - e^{-31}\sin\frac{\Phi}{2}, \end{aligned} \tag{4}$$

where Φ is the separation angle between the two vectors at their closest approach in their orbits. The BFF has its own complementary coordinate frame, (β_s, e_1, e_2, e_3) which is not related to the LFF by the usual Lorentz transformation which is discussed below. Equation (4) is written in the basis:

$$e_{31}^{\pm} = \frac{1}{\sqrt{2}}(e_3 \pm e_1). \tag{5}$$

The two cones are mirror images with equal phases and opposite frequencies. From these, the scalar and bivector, wedge parts are

$$\mathbf{S}_1 \cdot \mathbf{S}_3 = \cos\Phi, \qquad \mathbf{S}_1 \wedge \mathbf{S}_3 = e_2 \sin\Phi. \tag{6}$$

Hence, the geometric product is a unit quaternion, a rotor in 3D space, parameterized by Φ,

$$Q_B(\Phi) = \mathbf{S}_1\mathbf{S}_3 = \mathbf{S}_1 \cdot \mathbf{S}_3 + \mathbf{S}_1 \wedge \mathbf{S}_3 = \cos\Phi + e_2 \sin\Phi = e^{e_2\Phi}. \tag{7}$$

As the applied torque about 2 increases, the separation angle Φ decreases and the 1 and 3 cones approach. For an electron, the energy required to reach the limiting configuration is small, so the motion rapidly approaches the boundary where the cones touch at $\Phi = 0$. At this boundary, which is within their common 13 reflection plane, the two angular momenta, $\mathbf{S}_1$ and $\mathbf{S}_3$ intertwine. The two "hands", the $m = \pm 1$ blades form a double helix of mass with even parity. This defines the quantum domain where classical becomes quantum, as shown in Figure 1, right panel.

Isotropy is the absence of external polarization. In this case, the electron's state is $m = 0$, and exhibits only mass, m_e. It is EM-inert. In a polarizing field, the double helix is pulled apart so that one axis, with definite chirality, aligns with the field; charge and helicity also emerge and the aligned blade realizes one of the $m = \pm 1$ states, both of which are EM-active, [9].

The geometric product, Equation (7), suggests a natural partition: as Φ changes, the scalar mass part and the bivector's internal rotational part are balanced. This motivates the internal–external split developed in Section 3, where the fixed ratio between the external, field-coupled motion and the total rest energy is related to the FSC.

Equations (3)–(7) provide a complete BiSM description of classical spin which has a quantum limit. This replaces the need to postulate spin as the SM does.

Classical Rotor Lagrangian and FSC Partition

For completeness, we summarize [9] the ingredients needed to justify the energy split used here. In the classical domain, the bivector rotor is driven by a torque about the LFF Y–axis (the 2–axis). Part of this energy is transferred to the internal counter–precession of the 1 and 3 axes in the BFF. The classical Lagrangian follows from Equation (57) of [9], written as

$$\mathcal{L}_{\text{BiSM}} = -\frac{1}{4} G_{ab} G^{ab} + \frac{1}{2} M^2 A_a A^a + g J^\mu A_\mu. \tag{8}$$

Two distinct index sets are used. The BFF carries internal parity indices $a, b \in \{\beta_s, e_1, e_3\}$ with signature $(+,-,-)$; the LFF carries spacetime indices $\mu, \nu \in \{\beta, X, Y, Z\}$ corresponding to Minkowski space. This makes explicit the distinction between the internal rotor dynamics (indices a, b) and external interactions (indices μ, ν). Events occur simultaneously in both the BFF and the LFF, with the internal space projected onto the external one. This connection is established by a vierbein or tetrad field, see [14] page 483, and [15,16], which defines a local soldering map $e^\mu{}_a$ that projects BFF indices into LFF indices. In standard notation, for the electromagnetic four-potential transforms as,

$$A_a = e_a{}^\mu \, A_\mu, \qquad e_a{}^\mu \, e^b{}_\mu = \delta_a{}^b, \qquad e^a{}_\mu \, e_a{}^\nu = \delta_\mu{}^\nu. \tag{9}$$

Complementary spaces are geometrically distinct. The BFF describes the internal parity geometry of the bivector frame, while the LFF expresses its projection as an observable torque frame in spacetime. Because they occupy different domains, there is no global Lorentz transformation connecting them. The Lorentz group acts within a single spacetime manifold; it cannot map between internal and external spaces of opposite parity. Instead, $e^\mu{}_a$ provides a local correspondence that allows coupling terms such as $J^\mu A_\mu$ to be written while preserving the independence of the dual spaces.

Although this notation is unconventional, displaying mixed BFF and LFF components in Equation (8) keeps the geometry transparent. Conventionally, indices from the LFF are used for couplings, so the bivector rotor current J^μ interacts with the external potential A_μ, and the field-strength bivector tensor is defined by

$$G_{\mu\nu} \equiv \partial_\mu A_\nu - \partial_\nu A_\mu. \tag{10}$$

Thus A_μ and A_a are the components of the same physical potential written in the LFF and BFF bases respectively, related by Equation (9). Consequently any frame–independent scalar built from A is the same in either description, *e.g.* $A_a A^a = A_\mu A^\mu$. The electromagnetic field is $G_{\mu\nu} \equiv \partial_\mu A_\nu - \partial_\nu A_\mu$ in the LFF, with $G_{ab} = e_a{}^\mu e_b{}^\nu G_{\mu\nu}$ in the BFF, and $G_{ab} G^{ab} = G_{\mu\nu} G^{\mu\nu}$.

In the quantum limit [8,9], the same geometry separates these frames into two complementary domains. This bifurcation distinguishes the symmetry of the LFF (reflection) from that of the BFF (parity). The internal bivector motion in the BFF has definite even parity, while the external vector torque axis has definite odd parity. In the quantum domain, matter and force are separated; in the classical domain, they are geometrically mixed between two different frames. The classical domain becomes quantum as $\Phi \to 0$.

For the FSC, we need only the kinematic consequence of the rotor's internal geometry. The projection of the internal motion from the BFF to the LFF is what becomes visible, and this cannot represent the full bivector dynamics. The internal BFF blades ($m = \pm 1$) in the $(1, 3)$ plane counter-precess at twice the laboratory torque frequency about axis 2, manifesting the double cover. We use this structure to partition the energy and separate the internal inertial energy of the rotor (BFF) from its electromagnetic coupling energy (LFF). The ratio of these two contributions, fixed by geometry and the double-cover relation, yields the FSC in the BiSM.

3. The Fine-Structure Constant

The empirical FSC is [17],

$$\alpha \equiv \frac{e^2}{4\pi\varepsilon_0 \hbar c} = 7.2973525693 \times 10^{-3} \approx \frac{1}{137.036}. \tag{11}$$

This section shows that the same geometry that fixes the inertial and EM rings also fixes the share of energy available to each. No renormalization is required because the BiSM electron has intrinsic physical scales $(\bar{\lambda}_C, r_e)$. These provide natural ultraviolet bounds, in contrast to the SM, where divergences are removed by renormalization [18–20]. Low-energy quantities, including α, are obtained here without ad hoc cutoffs.

Write the rotational energies in the usual rigid-body form, $E_{\text{rot}} = \frac{1}{2} I \omega^2$, with I_V the effective moment of inertia for the laboratory vector motion and I_B for the internal bivector motion. According to Equation (1), this implies that

$$\alpha = \frac{E_V}{E_V + E_B} \tag{12}$$

The inertial ring is identified with reduced Compton length, $\bar{\lambda}_C$, which we take as the ring radius. Likewise, the laboratory coupling ring is the classical radius, r_e. The geometric ratio $\alpha = r_e/\bar{\lambda}_C$ is consistent with its experimental value. We can take a further step because the bivector's two blades counter-precess such that the internal blades carry twice the precession frequency of the torque axis; this is the origin of the factor of 4

$$\frac{E_{\text{V}}}{E_{\text{B}}} = \frac{I_{\text{V}}}{4I_{\text{B}}} \tag{13}$$

Assuming a rigid bivector, the ratio of the external energy from its helicity, and the internal energy of the bivector is fixed at the above ratio. From this, we parameterize the FSC by

$$\alpha = \frac{I_V}{I_V + 4I_B}. \tag{14}$$

Solving for the inertia ratio and using the value of α leads to the following:

$$\frac{I_B}{I_V} = \frac{1 - \alpha}{4\alpha} \approx 34.0, \qquad \frac{E_V}{E_B} \approx \frac{1}{136}. \tag{15}$$

These two values confirm that most stored rotational energy is internal while only a small external part is field-coupled. The values of $\bar{\lambda}_C$ and r_e are found using the following standard definitions [17,21,22]:

$$r_e = \frac{e^2}{4\pi\varepsilon_0 m_e c^2} \qquad \bar{\lambda}_C = \frac{\hbar}{m_e c} \tag{16}$$

Thus, α is a structural ratio in the bivector geometry

$$\alpha = \frac{r_e}{\bar{\lambda}_C} \tag{17}$$

In the BiSM, the electron's self-energy, E_V, is the portion of internal rotational energy that becomes available when the spin changes from the isotropic $m = 0$ state to a polarized $m = \pm 1$ state. Part of the confined rotational kinetic energy moves into field-coupled external motion on the perimeter. Thus, the $m = 0$ state is EM-inert, whereas the polarized states, $m = \pm 1$, are EM-active; the required energy is "self" because it originates in the electron's own structure and dynamics rather than from an external source.

From the LFF, spin is only the projection of the internal 2D rotor at the Compton scale and depends on the rotor's mass, m_e. The $m = \pm 1$ polarized states emerge from the internal static helix to generate the dynamic helicity degree of freedom in the LFF. There, it becomes field-coupled, enabling energy exchange at a scale set by r_e.

In summary, the internal transition $m = 0 \leftrightarrow m = \pm 1$ transfers a fixed share of the electron's structural energy content from internal confinement to external, field-coupled motion on the perimeter, governed by the quaternion, Equation (7).

$\bar{\lambda}_C$ sets inertia; r_e sets EM coupling.

Thomson Scattering

In the Thomson limit, $\hbar\omega \ll mc^2$, the Lorentz force exerts only a small classical acceleration, a, on the electron [23,24]. The radiated power scales as $P \propto a^2 \propto E^2$. The incident intensity also scales as $I \propto E^2$. Hence, the scattering cross-section, $\sigma \sim P/I$, is independent of the wave amplitude of ω. Physically, recoil is negligible, the electron behaves as a harmonically driven charge, and the result is fixed by geometry. The total Thomson cross-section is [21–24]

$$\sigma_T = \frac{8\pi}{3} r_e^2, \tag{18}$$

Equation (18) follows from integrating the classical dipole scattering pattern, $\frac{1}{2}(1 + \cos^2\theta)$ over solid angle [22,25]. Using the FSC α and the reduced Compton wavelength $\bar{\lambda}_C$, the classical radius can be written in the equivalent forms $r_e = \alpha\,\bar{\lambda}_C$. Substituting into Equation (18) yields

$$\sigma_T = \frac{8\pi}{3} \alpha^2 \bar{\lambda}_C^2 \tag{19}$$

making it clear that the area scale is the intrinsic Compton length suppressed by the square of the coupling α, and hence is small. The numerical value in Equation (19) agrees with the experiment by over 10^{-10} when evaluated with experimental CODATA constants [25,26].

$$\sigma_T = 6.652\,458\,7322 \times 10^{-29}\ m^2 \tag{20}$$

$$\sigma_T^{\text{exp}} = 6.652\,458\,7321 \times 10^{-29}\ m^2 \tag{21}$$

In the Thomson regime, the only available length is $r_e = \alpha\bar{\lambda}_C$, so no additional dimensionless parameter appears and σ_T is constant in ω. When $\hbar\omega \sim mc^2$, however, photon–electron energy–momentum exchange is non-negligible: the outgoing photon frequency shifts to the Compton scale, introducing the ratio $\hbar\omega/(mc^2)$ and leading to the Klein–Nishina cross section. The Thomson result is the $\hbar\omega/(mc^2) \to 0$ limit of Klein–Nishina, as expected from the correspondence principle [25,27,28].

Within the BiSM, the electron is a confined bivector rotor whose internal energy resides in the BFF, while only a thin electromagnetic perimeter is visible in the LFF. This share of the Compton-scale structure that can couple to external fields is fixed by α, so the

effective Thomson radius is $r_e = \alpha\,\bar{\lambda}_C$ and the observable area scales as $(\alpha\,\bar{\lambda}_C)^2$, reproducing Equation (19). Thus the smallness of σ_T has a direct physical meaning: external fields probe only an α-weighted rim of the bivector rotor; the bulk of the energy remains confined.

The Thomson cross-section is reproduced numerically by both the SM and the present BiSM. The distinction lies not in the value, but in the interpretation. The BiSM scale $r_e = \alpha\,\bar{\lambda}_C$ follows directly from the internal bivector geometry and the α-weighted energy share. This provides a mechanical origin for a quantity that, in conventional QED, is inserted phenomenologically. Thomson scattering offers a quantitative and physical success of the BiSM "energy-share" principle, and thereby provides deeper insight into Thomson Scattering. The intrinsic Compton length sets the scale, while α sets accessibility.

4. Discussion

The FSC quantifies how much of the electron's energy is externally EM-active versus internally inertial. With $E_{\text{rest}} = m_e c^2 \approx 511$ keV, the EM-active part is set by α

$$E_V = \alpha E_{\text{rest}} = \alpha m_e c^2 \approx 3.73 \text{ keV}. \tag{22}$$

This is a coupling or activation scale for the rim dynamics implied by the geometry, and not a discrete spectral line. Because the LFF carries odd parity and the BFF carries even parity, transitions between them are parity-forbidden, and thus do not produce radiative lines. The energy $\approx$ 3.73 keV corresponds to core-electron excitations in the few-keV regime. This is accessible to electron-induced X-ray experiments reviewed by [29,30], with the energy representing a natural geometric, or coupling, threshold between the inertial and electromagnetic domains carried by the bivector electron.

The internal BFF preserves the mass and spin of the electron and does not directly participate in EM coupling. Only a fraction of the electron's structure is visible to a field, while the bulk provides inertial stability. This view is consistent with the electron's capacity to transfer energy, momentum, and torque to a receptor [9]. Its electromagnetic component acts as an extended hand at the rim scale r_e, thereby conveying chirality and mediating the coupling, but without using much energy. Most of the mass–energy remains confined in the inertial ring at the Compton scale and is available to be transferred to a receptor to build structures [9]. Hence, the smallness of α reflects the confinement of energy in the internal bivector rather than an unexplained numerical coincidence.

This article follows as an application of the BiSM [9], and only focuses on establishing the geometric origin of α. These properties and other anomalies depend on the internal bivector dynamics related to the zbw and electron properties of charge and helicity [9]. These appear in forthcoming articles that rely on the structural results obtained here.

The SM treats the electron as a point excitation of a chiral spinor field and introduces the FSC as an empirical coupling parameter. Within QFT, no internal scale or structural mechanism fixes the value of α; its numerical value must be measured and renormalization is required to manage the ultraviolet divergences arising from the point-particle idealization. In contrast, the BiSM assigns the electron a definite internal geometry with intrinsic length scales, and the partition of inertial and electromagnetic degrees of freedom yields α as a structural ratio. While the SM successfully organizes and predicts a broad phenomenology, its point-like electron offers no geometric interpretation of the FSC. The present work, therefore, suggests that α may be understood not as a fundamental parameter to be fitted, but as a consequence of a deeper internal structure that classical and quantum descriptions share.

Note Added in Proof

After the preliminary acceptance of this paper, Santos and Fleury [31] reported a toroidal electromagnetic model of the electron in which circulating fields confined within a torus reproduce the QED values of charge, spin $\frac{1}{2}$, and magnetic moment. Their parameters were addusted to satisfy constraints, with a major torus radius $R_0 \simeq \lambda_C/\pi$ and a minor radius $r_0 \simeq \sqrt{\alpha}\, R_0$. Using the BiSM, the same geometry emerges naturally and is not imposed: the torus appears to represent the projection of the bivector rotor into spacetime $Cl(1,3)$ as described by the soldering map, Equation (9). The internal bivector radius r_e, (the classical radius here, defining the electromagnetic coupling), corresponds to the torus minor radius r_0. The external precession radius $\lambda_C/2\pi$ corresponds to inertia from the torus major radius R_0. The ratio $r_e/(\lambda_C/2\pi) = \alpha$ follows structurally from the coupling between confined and propagating energy, not from parameter fitting.

For the two approaches to coincide, the torus would need to be reinterpreted not as a physical ring of circulating fields but as the projection of a bivector rotor as discussed in Section Classical Rotor Lagrangian and FSC Partition. Both approaches recognize the need for intrinsic internal motion and thereby obviate the notion of a structureless point particle. While Santos and Fleury describe this motion as a phase circulating in a toroidal field confined to real space, the BiSM interprets it as the physical bivector rotation in the BFF, whose projection appears toroidal in the LFF. In this sense the two approaches converge, each replacing the point electron with a self-contained, dynamic structure.

Funding: This research received no external funding.

Data Availability Statement: No new data were created or analyzed in this study.

Conflicts of Interest: The author declares no conflicts of interest.

References

1. Eddington, A.S.; Whittaker, E.T. *Fundamental Theory*; The University Press: Cambridge, UK, 1946.
2. Dirac, P.A.M. A New Basis for Cosmology. *Proc. R. Soc. A* **1938**, *165*, 199–208. [CrossRef]
3. Feynman, R.P. *QED: The Strange Theory of Light and Matter*; Princeton University Press: Princeton, NJ, USA, 1985.
4. Feynman, R.P.; Leighton, R.B.; Sands, M. *The Feynman Lectures on Physics*; Addison-Wesley: Boston, MA, USA, 1964; Volume 1.
5. Morel, L.; Yao, Z.; Cladé, P.; Khélifa, S.G. Determination of the fine-structure constant with an atom-interferometric measurement of the recoil velocity of rubidium. *Nature* **2020**, *588*, 61–65. [CrossRef] [PubMed]
6. Parker, R.H.; Yu, C.; Zhong, W.; Estey, B.; Müller, H. Measurement of the fine-structure constant as a test of the Standard Model. *Science* **2018**, *360*, 191–195. [CrossRef] [PubMed]
7. Cladé, P.; GuellatiKhélifa, S. The fine structure constant α and the ratio h/m. *Comptes Rendus Phys.* **2019**, *20*, 77–92. [CrossRef]
8. Sanctuary, B. Quaternion Spin. *Mathematics* **2024**, *12*, 1962. [CrossRef]
9. Sanctuary, B. The Classical Origin of Spin: Vectors Versus Bivectors. *Axioms* **2025**, *14*, 668. [CrossRef]
10. Doran, C.; Lasenby, J. *Geometric Algebra for Physicists*; Cambridge University Press: Cambridge, UK, 2003.
11. Compton, A.H. A Quantum Theory of the Scattering of X-rays by Light Elements. *Phys. Rev.* **1923**, *21*, 483–502. [CrossRef]
12. Hestenes, D. The zitterbewegung interpretation of quantum mechanics. *Found. Phys.* **1990**, *20*, 1213–1232. [CrossRef]
13. Goldstein, H. *Classical Mechanics*; Addison-Wesley Publishing Compangy, Inc.: Reading, MA, USA, 1950; ISBN: 0-201-02510-8.
14. Carroll, S.M. *Spacetime and Geometry*; Cambridge University Press: Cambridge, UK, 2019.
15. Nakahara, M. *Geometry, Topology and Physics*, 2nd ed.; CRC Press: Boca Raton, FL, USA, 2003. [CrossRef]
16. Wald, R.M. *General Relativity*; University of Chicago Press: Chicago, IL, USA, 2024.
17. CODATA 2022 Recommended Values of the Fundamental Physical Constants, National Institute of Standards and Technology (NIST) Web Database. Available online: https://physics.nist.gov/cuu/Constants/ (accessed on 1 August 2025).
18. Wilson, K.G. Renormalization group and critical phenomena. I. Renormalization group and the Kadanoff scaling picture. *Phys. Rev. B* **1971**, *4*, 3174. [CrossRef]
19. Pauli, W.; Villars, F. On the invariant regularization in relativistic quantum theory. *Rev. Mod. Phys.* **1949**, *21*, 434. [CrossRef]
20. Doplicher, S.; Fredenhagen, K.; Roberts, J.E. The quantum structure of spacetime at the Planck scale and quantum fields. *Commun. Math. Phys.* **1995**, *172*, 187–220. [CrossRef]
21. Griffiths, D. *Introduction to Elementary Particles*; John Wiley & Sons: Hoboken, NJ, USA, 2009; pp. 59–60, ISBN 978-3-527-40601-2.

22. Jackson, J.D. *Classical Electrodynamics*, 3rd ed.; Wiley: Hoboken, NJ, USA, 1999; Sections 14–16.
23. Damm, H.; Pasch, E.; Dinklage, A.; Baldzuhn, J.; Bozhenkov, S.A.; Brunner, K.J.; Winters, V. First results from an event synchronized—High repetition Thomson scattering system at Wendelstein 7-X. *J. Instrum.* **2019**, *14*, C09037. [CrossRef]
24. Geltman, S. *Topics in Atomic Collision Theory*; Academic Press: Cambridge, MA, USA, 2013; Volume 30.
25. Rybicki, G.B.; Lightman, A.P. *Radiative Processes in Astrophysics*; John Wiley & Sons: Hoboken, NJ, USA, 2024.
26. Mohr, P.J.; Taylor, B.N. CODATA recommended values of the fundamental physical constants: 1998. *J. Phys. Chem. Ref. Data* **1999**, *28*, 1713–1852. [CrossRef]
27. Heitler, W. *The Quantum Theory of Radiation*; Courier Corporation: North Chelmsford, MA, USA, 1984.
28. Klein, O.; Nishina, Y. Über die Streuung von Strahlung durch freie Elektronen nach der neuen relativistischen Quantendynamik von Dirac. *Zeitschrift Physik* **1929**, *52*, 853–868. [CrossRef]
29. Egerton, R.F. *Electron Energy-Loss Spectroscopy in the Electron Microscope*, 4th ed.; Springer: Berlin/Heidelberg, Germany, 2021.
30. Rehr, J.J.; Ankudinov, A.L. Progress in the theory and interpretation of X-ray spectra. *Coord. Chem. Rev.* **2005**, *249*, 131–140. [CrossRef]
31. dos Santos, C.A.M.; Fleury, M.J.J. An electromagnetic model of the electron. *Ann. Fond. Louis Broglie* **2025**, *49*, 1–17.